URSI GASS 2021, Rome, Italy, 28 August - 4 September 2021

Microwave imaging for liver thermal ablation monitoring: developing an experimental set-up

Mengchu Wang* (1),(2), Rosa Scapaticci(1), Lorenzo Crocco(1), and Marta Cavagnaro(1),(2)
(1) CNR-IREA National Research Council of Italy, Institute for Electromagnetic Sensing of Environment, Napoli, Italy
(2) DIET, Sapienza University of Rome, Rome, Italy

Abstract

Thermal ablation has been recognized as an effective method for liver malignancy treatment. The clinical difficulties lie in monitoring the treatment process in real-time. In recent years, microwave imaging has been proposed as a modality with out-standing features such as non-ionizing nature, cost-effective, and capable of real-time monitoring. In this respect, in this contribution, a low-complexity experimental set-up for the experimental assessment of microwave imaging system for liver ablation monitoring is proposed and numerically assessed. The reconstruction of images inside the liver shows that it is possible to localize the ablation zone in the abdomen phantom during the thermal ablation treatment. The results of this study lay the foundations for the experimental assessment of microwave imaging systems for thermal ablation monitoring.

1 Introduction

Liver cancer is a malignancy occurring at an increasing rate per year around the world [1]. Untreated liver cancer leads to a patient mortality rate of approximately 100% within 5 years [2]. For quite a long time, conventional therapies like chemotherapy, radiation therapy, and surgical resection were considered to be effective methods to treat liver cancer [2]. However, increasing numbers of untreatable patients lead to the development of alternative treatments, as radio and microwave thermal ablation [3]. Thermal ablation aims at significantly increasing or decreasing the temperature in the area under treatment to induce irreversible cellular injury [4]. It proved to be an effective treatment with a minimum invasive approach [5].

Over the years, conventional imaging modalities such as ultrasound (US), computed tomography (CT), magnetic resonance imaging (MRI) have been used for thermal ablation planning on the clinical side [6]. However, no feasible modality has been developed for real-time monitoring of the ablation treatment process on the clinical side [6]. Indeed, at present, all the above cited techniques show some disadvantages that make the treatment monitoring heavily dependent on the experience of the clinician. Accordingly, the clinical challenge demands an alternative approach for monitoring the thermal ablation treatment.

Microwave imaging (MWI) is a technique that was proposed for medical diagnostic in recent years [7]. In comparison with the imaging modalities mentioned above, it shows the attractive characteristics of being non-ionizing, cost-effective, and based on compact-size systems [8]. In [9] a single-view mono-static MWI system for liver ablation monitoring was presented. The successful outcome showed that MWI is capable of providing real-time monitoring of thermal ablation.
In this paper, a simple set-up mimicking the human abdomen with a thermally ablated area into the liver is proposed and numerically assessed. The proposed set-up should allow performing experiments to design and optimize a microwave imaging system for liver ablation monitoring. To this end, an analysis is performed about the capability of a multi-view multi-static MWI array to locate an area of thermal ablated tissue within the simplified model of the human abdomen. The study is performed comparing images reconstructed from noise-free datasets and noisy datasets.

2 Methodology

Following the design guideline in [10], a low-complexity experimental set-up to simulate a microwave imaging system was proposed in this study, see Figure 1 (a). Here, 7 compact Vivaldi antennas were immersed inside a coupling medium (ε_r=23, σ=0.07 S/m) and placed close to an abdomen phantom. The distance between antennas is 23mm, each antenna acting both as transmitter and receiver. The frequency band is 0.5-2GHz. The selection of the coupling medium dielectric properties and the frequency band was based on the numerical analysis presented in [10]. It is a trade-off between electromagnetic penetration depth and imaging resolution. In fact, the selected properties proved to be capable of maximizing the electromagnetic power deliver to the liver [10].
To properly evaluate the performance of the microwave imaging system for monitoring liver thermal ablation, it is important to choose a phantom close to the abdomen

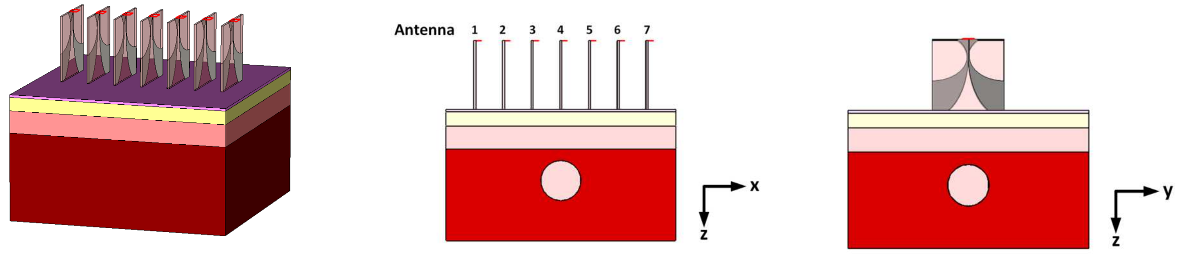

(a) (b) (c)

Figure 1 Proposed arrangement for the microwave imaging system experimental set-up: (a) perspective view, (b) x-z plane, (c) y-z plane

region. The proposed phantom consists of four planar layered tissues: skin, fat, muscle, and liver, with their thickness based on average statistics: 2.3mm, 12.2mm, 20.2mm, 80mm, respectively [11][12]. The dielectric properties of the tissue are based on the frequency-dependent single-pole Cole-Cole model [13]. The overall dimension of the abdomen phantom is 200 × 200 × 114.7 mm^3 (x-y-z-axis). A spherical target, whose diameter is 35mm, was placed inside the liver tissue to represent the ablation zone. The target was located 10mm beneath the muscle-liver interface, and in the center of the liver tissue (x-y plane), see Figure 1(b) and Figure 1 (c). The dielectric properties of the ablation zone are ε_r=26.67, σ=1.27 S/m at 2.45 GHz [14].

The algorithm used for the reconstruction of the images is the truncated singular value decomposition (TSVD) [9]. TSVD is an algorithm in the form of a regularization scheme; it is frequently used in solving small and medium-sized linear ill-posed problems [15]. TSVD is capable of real-time imaging since the computationally-intensive part is run off-line before data acquisition [9].

The linear reconstruction of the image is based on the differential signal calculated from two measurements in the region of interest (ROI): the measurement in the pre-ablation state and the measurement during/post-ablation. Such a differential signal is denoted as Δy, which is the consequence of the scattering field from the ablated area. and it has the following expression [16]:

$$\Delta y(r_p, r_q) = \frac{-j\omega\varepsilon_b}{4} \int_R E_i\left(r_p, r\right) \cdot E(r, r_q) \cdot \Delta x(r) dr \quad (1),$$

Where R is the region of interest, i.e., the imaging part, r_p and r_q are the positions of Rx and Tx antennas, ω = 2πf is the angular frequency, ε_b is the permittivity of the (not-homogeneous) background, i.e., the permittivity map of the ROI before the ablation treatment, E_i is the incident electric field, radiated by the antenna in the ROI before the ablation treatment, and E is the total field in the ROI after the ablation. Δx is the electrical contrast due to the changes in the dielectric properties induced by the ablation of the liver tissue.

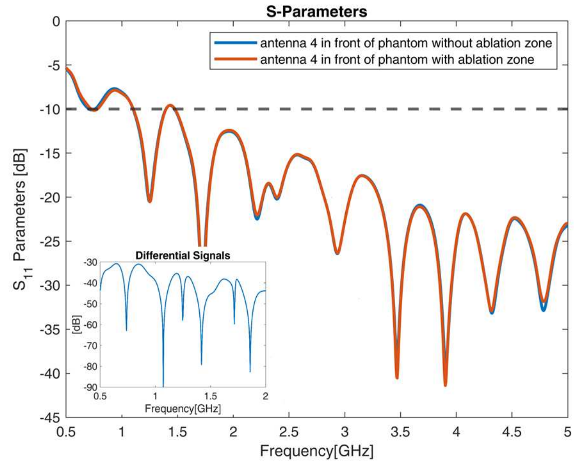

Figure 2 Simulated S11 parameters of antennas 4 in front of different phantoms

In the proposed circumstances, the post-ablation area behaves like a small scatterer located in the ROI. Its permittivity contrast with reference to the background medium (liver, in this case) is quite low. As a consequence, it is possible to use a distorted Born approximation which allows assuming that the incident field is equivalent to the total field $E_i(r_p, r) \cong E(r, r_q)$. So Δy becomes linearly dependent on Δx. Therefore, equation (1) can be written in a compact form:

$$\Delta y = K \cdot \Delta x \quad (2),$$

here K is the linear integral operator, mapping from the space Δx to Δy, represented as:

$$K \cong \frac{-j\omega\varepsilon_b}{4} \int_R E_i\left(r_m, r_p\right) \cdot E_i\left(r_m, r_q\right) \quad (3),$$

with $r_m \in R$. The incident field is calculated through the forward modeling of the system, evaluating the electromagnetic field radiated by the 7 antennas positioned in front of the abdomen phantom in the absence of the ablation zone. In this work, the calculation was performed through CST MW Studio® (Dassault Systèmes, France). CST is a software based on the finite integration technique applied to Maxwell's curl equation in the time domain. It is a marching in time scheme that

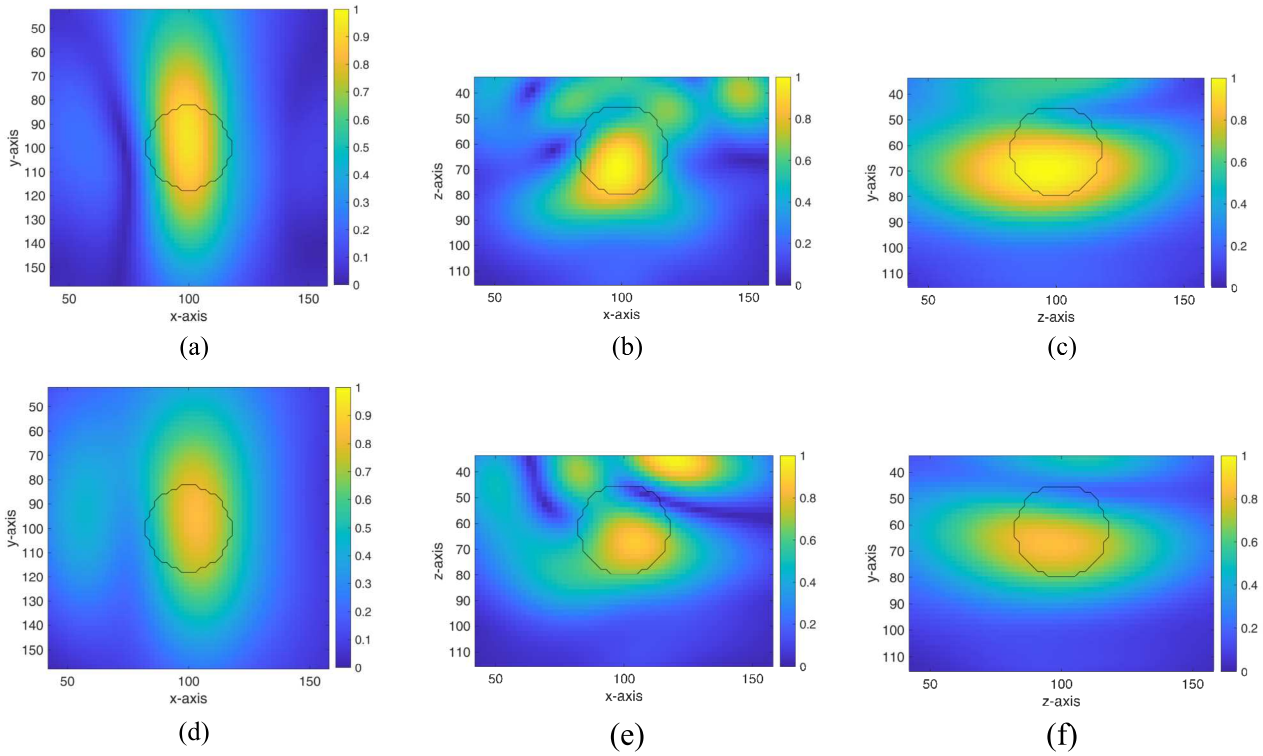

Figure 3 Reconstructed images inside the liver tissue on three orthogonal planes (reference system in Figure 1). Panels (a),(b),(c) refer to a noise-free dataset; panels (d),(e),(f) refer to a dataset with Gaussian noise SNR= 35 dB

simulates the propagation and interaction of electromagnetic waves in the region of interest [17].

To solve eq. (2) by TSVD, the singular value decomposition of K is represented as [15]:

$$\mathrm{K} = \mathrm{U} \cdot \sum \cdot \mathrm{V}^T \quad (4),$$

where U is the matrix of the left singular vectors of K, V is the matrix of the right singular vectors, and $\sum$ is a diagonal matrix of the singular values. The singular values σ_i in K are real and placed in decreasing order: $\sigma_1 \geq \sigma_2 \geq \cdots \geq 0$. Finally, the imaging problem is solved via the inversion of equation (2) as [15]:

$$\Delta x = K^{\dagger} \cdot \Delta y = \sum_{\sigma i \neq 0} \frac{1}{\sigma i} (u_i{}^T \cdot \Delta y) v_i \quad (5),$$

where $K^{\dagger}$ represents the inverse of the operator K, and σ_i are the singular values that decrease as integer i increase. Because in practical cases, the noise in Δy is inevitable, the division by a small singular value σ_i could lead to a large error in Δx. Therefore, a regularization scheme is necessary. It can be introduced in equation (5), as,

$$\Delta x_m = K^{\dagger}{}_m \cdot \Delta y = \sum_{\sigma_i \geq \sigma_m} \frac{1}{\sigma i} (u_i{}^T \cdot \Delta y) v_i \quad (6),$$

$K^{\dagger}{}_m$ is the regularized scattering operator, and m acts as a regularization parameter. In TSVD, the value of m is often properly chosen as a trade-off between the accuracy and the stability of the approximation, as larger m leads to higher accuracy but the stability of the problem is reduced accordingly [15].

3 Results and Discussion

Figure 2 shows the simulated S_{11} parameters of antenna 4 (center of the array) when it is positioned in front of the phantom in the absence of the ablation zone and in the presence of the ablation zone. The quantitative difference in the frequency band of interest (0.5-2 GHz), shown in the inset of the figure, evidences that the differential signal level varies between -30 and -40dB.
The reconstructed images inside the liver tissue along three orthogonal planes are given in Figure 3 (reference system in Figure 1). In the figure, the reconstructed images achieved using both a noise-free dataset and a dataset with Gaussian noise (SNR=35dB) are shown. The processed data are reported as the normalized amplitudes of the differential contrast. The black contours indicate the actual position of the ablated area. From the figure, it can be noted that for both cases, a highly overlap between the actual position and the reconstruction of the ablation zone is obtained. As expected, the target is less pronounced, but still evident, in the noisy figure. The results in Figure 3 show that the system is capable of providing localization of the ablation zone inside the liver. Moreover, such a system is robust against a Gaussian noise whose SNR level is 35dB, which is expectable in a real experimental environment.

4 Conclusion and Future Work

This paper presents the numerical assessment of a multi-view multi-static MWI system for real-time monitoring of thermal ablation of liver tumors. The aim of the work was to prove the usability of a simple set-up mimicking the human abdomen to conduct MWI experiments. The reconstructed images, even in the presence of noise, show that a simple layered phantom is useful for conducting MWI experiments. Additionally, the simple structure should allow changing the thermally ablated area location and properties.
Future work foresees the realization of the experimental set-up, i.e., the phantom, the coupling medium, and antennas. Moreover, efforts can be made to modify the antenna array arrangement and increase the number of antenna elements to improve the imaging resolution.

5 Acknowledgements

This work was supported by the EMERALD project funded from the European Union's Horizon 2020 research and innovation program under the Marie Skłodowska-Curie grant agreement No. 764479.

6 References

[1] F. X. Bosch, J. Ribes, M. Díaz, and R. Cleries, "Primary liver cancer: "worldwide incidence and trends," *Gastroenterology*, vol. 127, no. 5, pp. S5–S16, 2004.

[2] J. P. McGahan, & G. D. Dodd III, "Radiofrequency ablation of the liver: current status", *American Journal of Roentgenology*, 176(1), 3-16, 2001.

[3] M. Ahmed, C. L. Brace, F. T. Lee Jr, & S. N. Goldberg, "Principles of and advances in percutaneous ablation". *Radiology,* 258(2), 351-369, 2011.

[4] C. L. Brace, "Radiofrequency and microwave ablation of the liver, lung, kidney, and bone: what are the differences?". *Current problems in diagnostic radiology*, 38(3), 135-143, 2009.

[5] C. J. Simon, D. E. Dupuy, and W. W. Mayo-Smith, "Microwave ablation: principles and applications," *Radiographics*, vol.25, no. suppl 1, pp. S69–S83, 2005

[6] M. Ahmed, L.Solbiati, C. L. Brace, D. J. Breen, M. R. Callstrom, J. W. Charboneau, ... & S. N. Goldberg, "Image-guided tumor ablation: standardization of terminology and reporting criteria—a 10-year update", *Radiology*, 273(1), 241-260, 2014.

[7] N. K. Nikolova, "Introduction to microwave imaging", *Cambridge University Press*, 2017.

[8] M. Pastorino, "Microwave imaging", *JohnWiley & Sons*, vol.208, 2010.

[9] R. Scapaticci, V. Lopresto, R. Pinto, M. Cavagnaro, and L. Crocco, "Monitoring thermal ablation via microwave tomography: An ex vivo experimental assessment," *Diagnostics*, vol.8, no.4, p.81, 2018.

[10] M. Wang, L. Crocco and M. Cavagnaro, "On the Design of a Microwave Imaging System to Monitor Thermal Ablation of Liver Tumors," in *IEEE Journal of Electromagnetics, RF and Microwaves in Medicine and Biology*, 2021.

[11] I. G. Zubal, C. R. Harrell, E. O. Smith, Z. Rattner, G. Gindi, and P. B. Hoffer, "Computerized three-dimensional segmented human anatomy," *Medical physics*, vol.21, no.2, pp.299–302, 1994.

[12] O. Akkus, A. Oguz, M. Uzunlulu, M. Kizilgul et al., "Evaluation of skin and subcutaneous adipose tissue thickness for optimal insulin injection," *J Diabetes Metab*, vol.3, no.8, p.2, 2012.

[13] S. Gabriel, R. Lau, and C. Gabriel, "The dielectric properties of biological tissues: Iii. Parametric models for the dielectric spectrum of tissues," *Physics in medicine & biology*, vol.41, no.11, p.2271, 1996.

[14] V. Lopresto, R. Pinto, G. A. Lovisolo, and M. Cavagnaro, "Changes in the dielectric properties of ex vivo bovine liver during microwave thermal ablation at 2.45 GHz," *Physics in Medicine & Biology*, vol.57, no. 8, p.2309, 2012.

[15] X. Chen, "Computational methods for electromagnetic inverse scattering", *New York: John Wiley & Sons*, 2018.

[16] R. Scapaticci, J. Tobon, G. Bellizzi, F. Vipiana, & L. Crocco, "Design and numerical characterization of a low-complexity microwave device for brain stroke monitoring", *IEEE Transactions on Antennas and Propagation*, 66(12), 7328-7338, 2018

[17] D. B. Davidson, Computational electromagnetics for RF and microwave engineering, *Cambridge University Press*, 2010.